ARTICLES
PUBLISHED ONLINE: 17 MAY 2009 | DOI: 10.1038/NMAT2460
nature materials

A highly ordered nanostructured carbon–sulphur cathode for lithium–sulphur batteries

Xiulei Ji, Kyu Tae Lee and Linda F. Nazar*

The Li–S battery has been under intense scrutiny for over two decades, as it offers the possibility of high gravimetric capacities and theoretical energy densities ranging up to a factor of five beyond conventional Li-ion systems. Herein, we report the feasibility to approach such capacities by creating highly ordered interwoven composites. The conductive mesoporous carbon framework precisely constrains sulphur nanofiller growth within its channels and generates essential electrical contact to the insulating sulphur. The structure provides access to Li^+ ingress/egress for reactivity with the sulphur, and we speculate that the kinetic inhibition to diffusion within the framework and the sorption properties of the carbon aid in trapping the polysulphides formed during redox. Polymer modification of the carbon surface further provides a chemical gradient that retards diffusion of these large anions out of the electrode, thus facilitating more complete reaction. Reversible capacities up to 1,320 mA h g^{-1} are attained. The assembly process is simple and broadly applicable, conceptually providing new opportunities for materials scientists for tailored design that can be extended to many different electrode materials.

Safe, low-cost, high-energy-density and long-lasting rechargeable batteries are in high demand to address pressing environmental needs for energy storage systems that can be coupled to renewable sources[1,2]. These include wind, wave and solar energy, as well as regenerative braking from vehicular transport. With production of oil predicted to decline, and the number of vehicles and their pollution impact increasing globally, a transformation in transportation economy is inevitable given that we live in a carbon-constrained world. One of the most promising candidates for storage devices is the lithium–sulphur cell. Under intense scrutiny for well over two decades, the cell in its simplest configuration consists of sulphur as the positive electrode and lithium as the negative electrode[3,4]. It differs from conventional lithium-ion cells, which operate on the basis of topotactic intercalation reactions: reversible uptake of Li ions and electrons in a solid with minimal change to the structure. They typically use a lithium transition-metal oxide or phosphate as a positive electrode (cathode) that de/re-intercalates Li^+ at a high potential with respect to the carbon negative electrode (anode). As the reaction is topotactic at both electrodes, the charge storage capability is inherently limited to about 300 mA h g^{-1} for any prospective system, and maximum capacities observed so far are 180 mA h g^{-1} with high power characteristics having been reported[5]. The lithium–sulphur cell operates quite differently. The redox couple, described by the reaction $S_8 + 16Li \leftrightarrow 8Li_2S$ lies near 2.2 V with respect to Li^+/Li^o, a potential about 2/3 of that exhibited by conventional positive electrodes[6]. However, this is offset by the very high theoretical capacity afforded by the non-topotactic 'assimilation' process, of 1,675 mA h g^{-1}. Thus, compared with intercalation batteries, Li–S cells have the opportunity to provide a significantly higher energy density (a product of capacity and voltage). Values can approach 2,500 W h kg^{-1} or 2,800 W h l^{-1} on a weight or volume basis respectively, assuming complete reaction to Li_2S (refs 7, 8).

Despite its considerable advantages, the Li–S cell is plagued with problems that have hindered its widespread practical realization. These arise from the fact that all components of the cell must be addressed as a whole, including the interfaces between them. Sulphur or sulphur-containing organic compounds are highly electrically and ionically insulating[9]. To enable a reversible electrochemical reaction at high current rates, the sulphur must maintain intimate contact with an electrically conductive additive. Various carbon–sulphur composites have been used for this purpose, but they have limitations owing to the scale of the contact area. Typical reported capacities are between 300 and 550 mA h g^{-1} at moderate rates[10]. To make a sulphur-containing cathode ionically conductive, liquid electrolytes are used that act not only as a charge transport medium but also as ionic conductors within the sulphur-containing cathode[11]. This presents difficulties of electrolyte access. Another major hurdle is capacity degradation on repeated discharge–charge of the cell. This is mainly due to the high solubility of the polysulphide anions formed as reaction intermediates in both discharge and charge processes in the polar organic solvents used in electrolytes[12]. During cycling, the polysulphide anions can migrate through the separator to the Li negative electrode whereupon they are reduced to solid precipitates (Li_2S_2 and/or Li_2S), causing active mass loss. In addition, the solid product that extensively precipitates on the surface of the positive electrode during discharge becomes electrochemically irreversible, which also contributes to active mass loss[13].

In response to these considerable challenges, novel advances in materials design such as new electrolytes[14–17] and protective films for the lithium anode have been developed[18–20]. Combinations of electrolyte modification, additives and anode protection have resulted in some promising results, although rates are not given[21]. Much of the difficulty still remains at the cathode, where the lack of breakthroughs has led to some cell configurations in which all of the sulphides are solubilized (so-called 'catholyte' cells)[22]. In the opposite approach, that is, to contain the sulphides, some interesting cathode developments have been reported recently[23–26]. However, they still fall short of the mark for practical electrochemical performance. They include, for example, the fabrication of disordered mesoporous carbon/sulphur 50:50 composites in conjunction with ionic liquid electrolytes; systems that achieve high initial capacity, but suffer extensive capacity

University of Waterloo, Department of Chemistry, Waterloo, Ontario N2L 3G1, Canada. *e-mail: lfnazar@uwaterloo.ca.

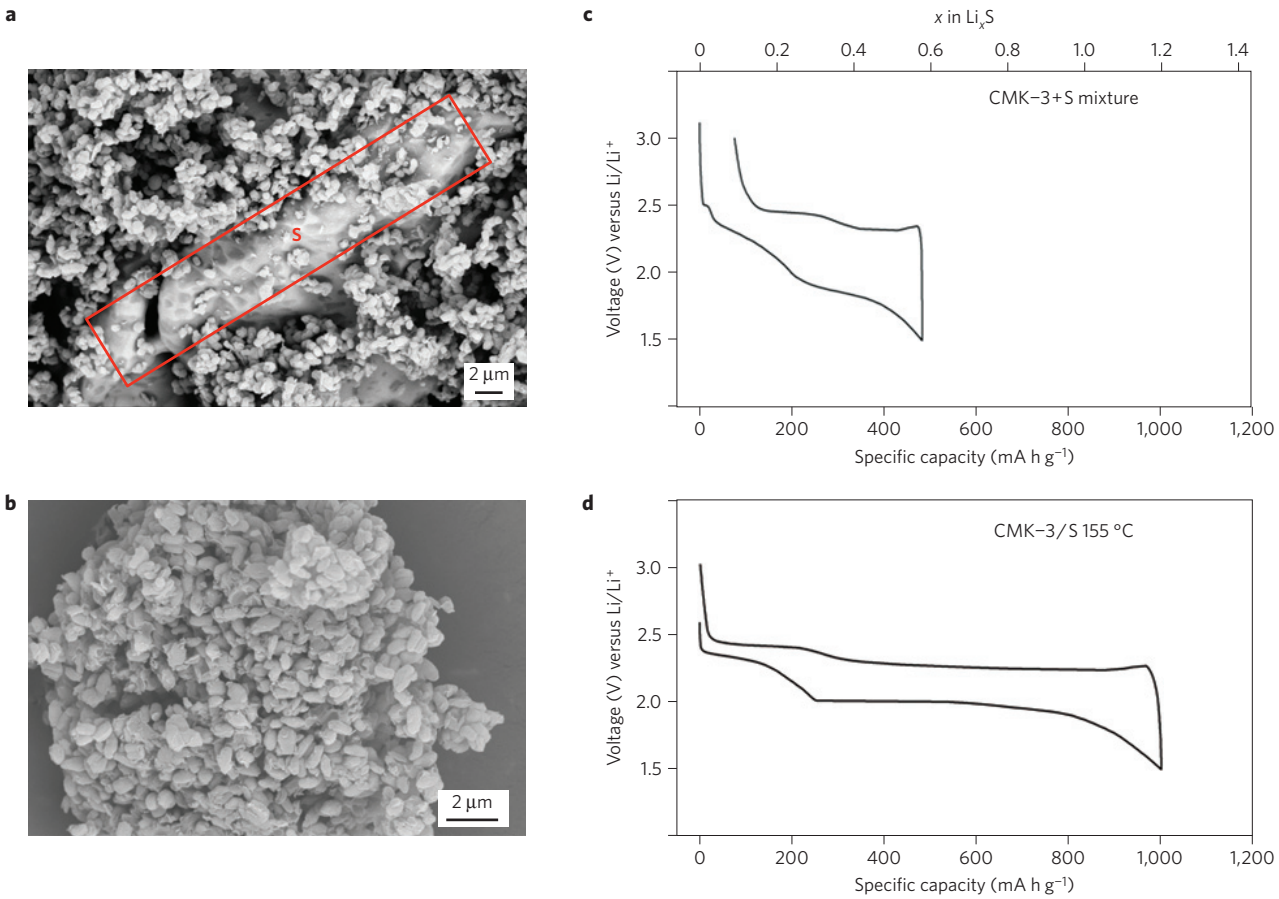

Figure 1 | SEM images of CMK-3/sulphur, and its electrochemical characterization. a, Mixture of CMK-3 and elemental sulphur before heating. **b**, CMK-3/S heated at 155 °C, showing the disappearance of the sulphur mass indicated by the red rectangle in **a**. **c**,**d**, Comparison of the galvanostatic discharge–charge profiles of the first cycles of the carbon–sulphur composites shown in **a**,**b**, at a current rate of 168 mA g^{-1}. The marked increase in capacity in **d** is due to the encapsulation effect.

fading[17]. Composites with sulphur embedded in conducting polymers have shown some promising results[27]. However, a large polarization was observed, resulting in a very low operating voltage that reduces the energy density of cells. The loading of active mass in the S-polymer composite is also limited (less than 55 wt%) owing to the low surface area of the conducting polymer. Here, we demonstrate that cathodes based on nanostructured sulphur/mesoporous carbon materials can overcome these challenges to a large degree, and exhibit stable, high, reversible capacities (up to 1,320 mA h g^{-1}) with good rate properties and cycling efficiency.

Our proof-of-concept studies are based on CMK-3, the most well-known member of the mesoporous carbon family, although they are not limited to this material. Highly ordered mesoporous carbons exhibit a uniform pore diameter, very high pore volume, interconnected porous structure and can exhibit high conductivity[28,29]. They, and their oxide analogues[30,31], have attracted much attention recently as nanoscale electrode materials in Li batteries[32,33], as supercapacitors and as supports for proton-exchange-membrane fuel-cell catalysts[34]. CMK-3 was synthesized by a nanocasting method that uses silaceous SBA-15 as a hard template. The resulting replica comprises an assembly of hollow 6.5-nm-thick carbon rods separated by empty 3–4-nm-wide channel voids[35]. The channel space is spanned by carbon microfibres that prevent the collapse of the nano-architecture of the two-dimensional hexagonally ordered carbon rods. We tuned the synthesis of the CMK-3 to produce a short rod-like morphology, to optimize access to the mesoporous channels[36]. The CMK-3/sulphur composite was prepared following a simple melt-diffusion strategy. A 3:7 weight ratio mixture of CMK-3 and sulphur was heated just above the melting point of sulphur, where the viscosity is lowest[37]. The melt is imbibed into the channels by capillary forces, whereupon it solidifies and shrinks to form sulphur nanofibres that are in intimate contact with the conductive carbon walls.

The scanning electron microscopy (SEM) images in Fig. 1 reveal the changes in the mixture of CMK-3 and sulphur before and after heating. The bulk sulphur evident in the SEM image of the composite on initial mixing (Fig. 1a) largely disappears at 145 °C (see Supplementary Fig. S1), and completely disappears after heat treatment at 155 °C (Fig. 1b). Full incorporation of sulphur into the channels of CMK-3 occurs at this latter temperature. CMK-3 and sulphur are both hydrophobic materials, which accounts for the ready absorption of sulphur into the channel structure. The filling of the carbon channels with sulphur is corroborated by the transmission electron microscopy (TEM) image shown in Fig. 2a, along with the magnified image shown in Fig. 2b. The fibres have a similar diameter to that of the channels of the mesoporous carbon (3.3 nm), and a comparable diameter to the carbon nanorods that enclose them (6–7 nm). The filling of the pores with sulphur, of similar density to carbon, is also evident from the decrease in contrast in relation to CMK-3 itself (shown in the inset in Fig. 2b). The sulphur and carbon elemental maps (Fig. 2c, d) clearly demonstrate that sulphur is homogeneously distributed in the framework of the mesoporous carbon, with no significant fraction on the external surface. The marked diminution

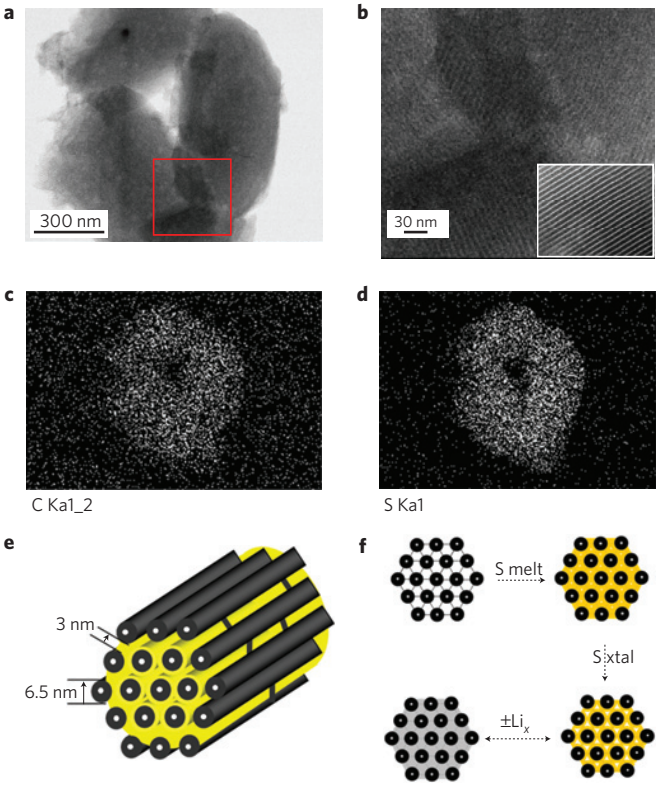

Figure 2 | TEM image and elemental maps of a CMK-3/S-155 composite particle and schematic diagrams of the structure and redox processes. **a**, CMK-3/S-155 composite particle. **b**, Image expansion corresponding to the area outlined by the red square in **a**, where the inset shows the TEM image for pristine CMK-3 at the same magnification. **c**,**d**, Corresponding carbon and sulphur elemental maps showing the homogeneous distribution of sulphur. **e**, A schematic diagram of the sulphur (yellow) confined in the interconnected pore structure of mesoporous carbon, CMK-3, formed from carbon tubes that are propped apart by carbon nanofibres. **f**, Schematic diagram of composite synthesis by impregnation of molten sulphur, followed by its densification on crystallization. The lower diagram represents subsequent discharging–charging with Li, illustrating the strategy of pore-filling to tune for volume expansion/contraction.

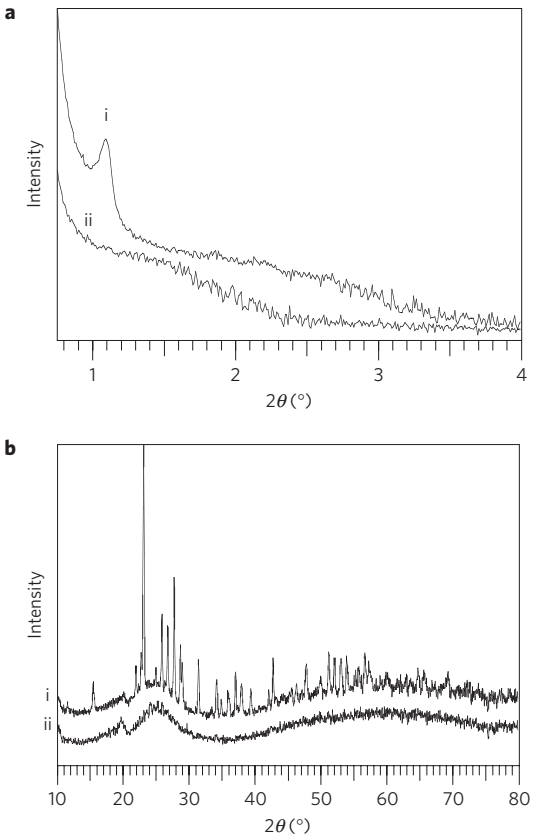

Figure 3 | XRD patterns of CMK-3/S before and after heating. **a**, Low-angle XRD patterns of a mixture of CMK-3 and sulphur before heating (i) and after heating at 155 °C (ii). The disappearance of the first peak is due to the loss of contrast on sulphur imbibition. **b**, Wide-angle XRD patterns of a mixture of CMK-3 and sulphur before heating (i) and after heating at 155 °C (ii), showing the complete incorporation of crystalline sulphur within the framework.

of the X-ray diffraction (XRD) peak (low-angle diffraction pattern, Fig. 3a) due to long-range order in CMK-3 is further proof of pore-filling, which is the result of the decrease in the scattering contrast (Fig. 3a)[38]. Comparing the wide-angle XRD patterns in Fig. 3b, the well-resolved peaks corresponding to bulk crystalline sulphur completely disappear after sulphur impregnation, and thermogravimetric analysis (TGA; Supplementary Fig. S2) shows the composites range up to 70 wt% sulphur. A schematic diagram illustrating the impregnation of the CMK-3 with sulphur is shown in Fig. 2e, showing the alignment of the channels in comparison with the inset of Fig. 2b. Note that most of the sulphur is contained within the interior of the pore structure, as the particles span hundreds of carbon channels in width. The average CMK-3 particle size is of the order of 1 μm (Fig. 1b).

Table 1 summarizes the physical characteristics of the CMK-3 and the CMK-3/S composite derived from Brunauer–Emmett–Teller (BET) and conductivity measurements. After imbibition of the sulphur in the channels, the pore size of the CMK-3/S composite decreases markedly, indicating that the channels of CMK-3 are partially filled. Along with the presence of residual micropores in the carbon wall structure[39], this allows ingress of electrolyte within the structure. Empty volume within the pores is also necessary to accommodate the uptake of Li ions, given by the reaction $S + 2Li \rightarrow Li_2S$, because of the lower density of Li_2S (1.66 g cm^{-3}) compared with sulphur. Note that the 70 wt% sulphur/composite ratio is less than the theoretical limit of 79 wt% sulphur/composite based on the pore volume of CMK-3 (2.1 cm^3 g^{-1}) and the density of liquidized sulphur (1.82 g cm^{-3}), and is precisely tuned for the volume expansion (see the Methods section). Using even lower S/carbon ratios provides less 'stuffed' structures and extra porosity, but at the expense of reduced active mass. Most importantly, the electrical conductivity of the composites (~0.2 S cm^{-1} for 70 wt% sulphur/composite) is the same as its mesoporous carbon counterpart. The insulating sulphur merely occupies the empty channels in the mesoporous carbon and does not block the electrical current transporting paths. Three-dimensional, multiple electronic contacts are provided by the numerous carbon interconnects that span the channels, as illustrated schematically in Fig. 2e, f (ref. 35).

Coin cells using a metallic Li anode were assembled to evaluate the materials. All of the capacity values in this article are calculated on the basis of sulphur mass. The first discharge–charge curve for a typical nanostructured CMK-3/S cathode is shown in Fig. 1d alongside its SEM image, and is compared with a simple physical (unheated) mixture of 7:3 weight ratio of sulphur and CMK-3 in Fig. 1c. The nanostructured composite exhibits an impressive capacity of 1,005 mA h g^{-1}. In contrast, the 'macro-mixture' exhibited a reversible capacity of 390 mA h g^{-1} (on average between 300 and 420 mA h g^{-1}), similar to that reported in the literature for C–S composites[10]. The capacity of CMK-3/S was

Table 1 | Physical characteristics of CMK-3 and the CMK-3/sulphur composite.

Samples	BET total surface area ($m^2\ g^{-1}$)	Pore volume ($cm^3\ g^{-1}$)	Micropore surface area ($m^2\ g^{-1}$)	BJH pore size (nm)	Conductivity ($S\ cm^{-1}$) (±0.02)
CMK-3	1976	2.1	152	3.33	0.20
CMK-3/S-70%	*46	*0.028	*5.1	1.1	0.21

BJH: Barrett–Joyner–Halenda. As it was not possible to follow the conventional protocol of evacuating the samples at 150 °C before BET measurements owing to the volatility of the sulphur, no pretreatment was used for CMK-3/S-70%. The possibility of water entrapment, and/or pore blockage in the predominantly micropore-containing CMK-3/S means that the values represent lower estimates (see the Methods section).

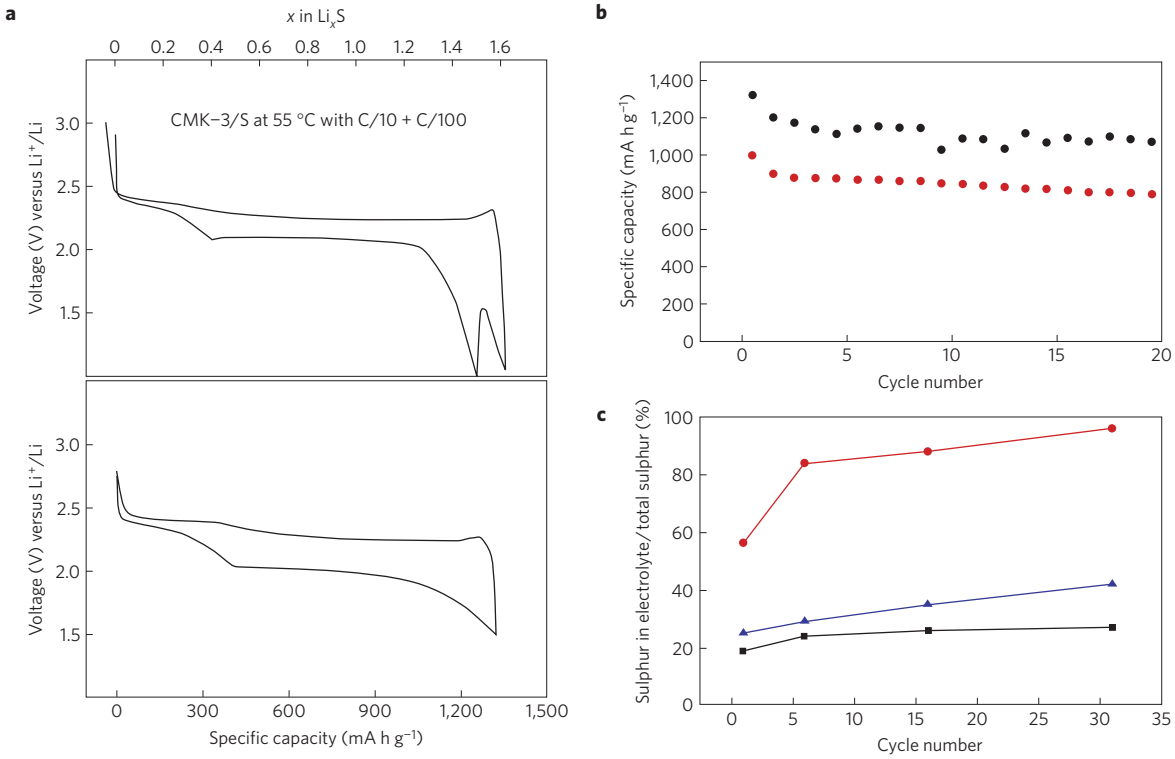

Figure 4 | Electrochemical characterization of PEG-coated CMK-3/S and comparison to reference materials. a, Lower panel: galvanostatic discharge–charge profile of PEG-modified CMK-3/S-155 recorded at room temperature at 168 mA g^{-1}. The reversible capacity of 1,320 mA h g^{-1} at room temperature is very close to that obtained for unmodified CMK-3/S obtained at elevated temperature under 'quasi-equilibrium' conditions shown in the upper panel (CMK-3/S-155 recorded at 55 °C at 168 mA g^{-1} on discharge to 1.0 V followed by quasi-equilibrium discharge at 16.8 mA g^{-1}). The slight overcharge in the latter case is due to dissolution of some polysulphide, which is minor even at these conditions. This also indicates that storage of the cell at partial or full discharge does not lead to significant capacity loss. **b**, Cycling stability comparison of CMK-3/S-PEG (upper points, in black) versus CMK-3/S (lower points, in red) at 168 mA g^{-1} at room temperature. **c**, Percentage of sulphur dissolution into the electrolyte from: the CMK-3/S-PEG composite cathode (black curve); from the CMK-3/S composite cathode (blue curve); a cathode made of a mixture of acetylene black carbon and sulphur with the exact same C/S ratio (red curve).

highly reproducible over many cells. The coulombic efficiency for CMK-3/S in the first discharge–charge cycle is 99.94% without any overcharge, with virtually no irreversibility. This indicates that a very low fraction of polysulphide anions diffuse into the electrolyte. The polarization was decreased by more than a factor of three, owing to the greatly enhanced electrical contact achieved in the nanostructure. Further unequivocal proof of the effectiveness of the contact arises from experiments in which the degree of S incorporation was varied. Nanostructured composites (CMK-3/S-145) with the same S/C ratio, but heated at 145 °C instead of 155 °C result in less complete diffusion of sulphur into the channels because of the higher viscosity at the lower temperature. These composites showed less utilization of sulphur (capacity of 780 mA h g^{-1}) in the first discharge sweep (see Supplementary Fig. S3), and an irreversible capacity of 50 mA h g^{-1} on charge. Complete imbibition prevents sulphur agglomerates on the external surface of the mesoporous framework that would have poorer electrical wiring of the conductive carbon phase. These results are superior to those reported for sulphur in contact with multi-walled carbon nanotubes. Such composites exhibit lower capacities and a large electrochemical hysteresis[23]. Although the sulphur is apparently confined in the carbon, the contact is limited owing to the relatively large diameter (~50 nm) of the multi-walled carbon nanotubes, and hence of the sulphur fibres within them. Thus, the efficiency of electron transfer to the sulphur mass and accessibility to the Li^+ electrolyte has a vitally important role in determining the electrochemical behaviour.

As seen in Fig. 1d, there are two plateaux in the discharge process. The first, which contributes a minor part to the overall capacity from 2.4 to 2.0 V, corresponds to the conversion from elemental sulphur (S_8) to Li polysulphide anions (Li_2S_x; where x is typically 4–5). The kinetics of this reaction is fast[40]. The second plateau at

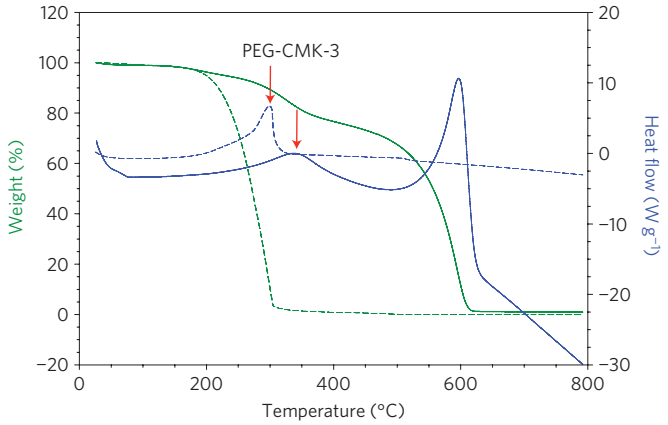

Figure 5 | TGA of PEG-modified CMK-3. TGA and differential scanning calorimetry curves recorded in air with a heating rate of 20 °C min^{-1}, for PEG-CMK-3 (solid lines), compared with PEG itself (dashed lines), showing the shift to higher temperature of the PEG release on bonding to the CMK-3 framework.

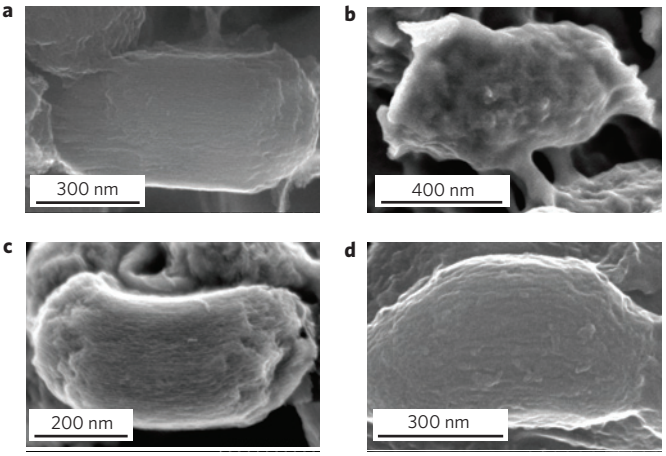

Figure 6 | Changes in surface morphology of CMK-3/S-155 versus PEG-modified CMK-3/S-155 on cycling. a,**b**, SEM images of CMK-3/S-155 before (**a**) and after (**b**) the 15th charge. **c**,**d**, SEM images of PEG-modified CMK-3/S before (**c**) and after (**d**) the 15th charge. Images show the effects of 'polymer protection' in inhibiting surface deposition.

around 2.0 V is due to the conversion of polysulphides to Li_2S_2 and then to Li_2S, which occurs at a much slower rate. As we achieve a nominal reversible capacity of $Li_{1.2}S$ in the nanostructured composite, we wanted to explore the limitations to full conversion. To gain a measure of the reversible capacity under conditions where the kinetics should be a minimal concern, we carried out discharge of the CMK-3/S cathode at 55 °C at 168 mA g^{-1} to a cutoff of 1.0 V, and allowed the voltage to relax to equilibrium. We then switched the discharge current to a rate of 16.8 mA g^{-1} to the end of discharge, and completed charge at 168 mA g^{-1}. The electrochemical profile is presented in Fig. 4a (upper panel). Under these close-to-equilibrium conditions of full discharge, we achieve a reversible capacity of 1,400 mA h g^{-1}—84% of the theoretical capacity (1,675 mA h g^{-1})—indicating that indeed, the kinetics of the last reaction step has a role in capacity limitation. The other factor could be a transport problem. There is progressively more limited accessibility of Li^+ ions and electrolyte to the sulphur mass towards the end of discharge because the pores become filled with insoluble Li_xS ($x = 1$–2)—even though at 70 wt% sulphur loading, there is sufficient space for the volume expansion based on the conversion of S to Li_2S. However, we observed that in doubling the rate from 168 to 336 mA g^{-1} (equivalent to C/5 rate), the capacity is reduced by only a small amount to 930 mA h g^{-1} (see Supplementary Fig. S4).

The mesoporous carbon clearly performs very well as a sulphur container. This is apparent from the small degree of overcharge even under rigorous (55 °C; C/100 discharge) conditions as shown in Fig. 4a. The complete lack of a sharp minimum in the discharge curve between the two plateaux, as observed by others and ascribed to supersaturation of the electrolyte with S^{2-} (refs 21, 41), is also indicative of the strong extent of sulphide containment in our case. Experiments were carried out to evaluate the degree of self-discharge, by taking the cell to a voltage of 2.1 V, holding it at the open-circuit voltage for 24 h and then completing discharge. The discharge capacity after relaxation was 5% less than the cell taken to full discharge without the open-circuit voltage step. However, this suggests that the framework still allows for some egress of dissolved sulphur species. We propose that the complex inner pathway and porous, absorptive carbon greatly retard the diffusion of the bulky polysulphide anions out from the channels into the electrolyte, but cannot entirely prevent it. This is evident by the very slow capacity fading shown in Fig. 4b (upper red points).

To further trap the highly polar polysulphide species, we adjusted the hydrophilicity of the carbon external surface after sulphur imbibition by functionalizing the surface with polyethylene glycol (PEG) chains of varying molecular weight. The attachment of the PEG to CMK-3 is evident by TGA (Fig. 5). The release of the PEG tethered to the CMK-3 occurs at 50 °C higher than in PEG itself owing to the ester bonds. The discharge–charge profile of CMK-3/S-PEG is shown in Fig. 4a (lower panel). Not only is the initial discharge capacity increased to 1,320 mA h g^{-1} (approaching the 'equilibrium' limit for CMK-3/S of 1,400 mA h g^{-1}), and the polarization decreased to low values, but no fading is observed in the second 10 cycles and the capacity is stabilized at 1,100 mA h g^{-1} on cycling (Fig. 4b, upper black points).

The entrapment of sulphur active mass on cycling in the polymer-modified CMK-3/S composite is demonstrated in Fig. 4c. To measure the degree of sulphur retention in the cathode, a 1.0 M $LiPF_6$ solution in a sulphur-free solvent, tetra(ethylene glycol) dimethyl ether (TEGDME), was used as the electrolyte. Glyme solvents are known for their excellent ability to dissolve polysulphides, and hence represent an 'aggressive' case. Compared with the cathode made of a mixture of sulphur and acetylene black that loses 96% of the total active mass into the electrolyte after 30 cycles, the polymer-modified composite shows significant retention of sulphur. Only 25% of the total active mass is solubilized in the electrolyte after 30 cycles. The polysulphide retention is also improved in relation to CMK-3/S. We believe that the effect of the PEG-functionalized surface is twofold. First, it serves to trap the polysulphide species by providing a highly hydrophilic surface chemical gradient that preferentially solubilizes them in relation to the electrolyte. Second, by limiting the concentration of the polysulphide anions in the electrolyte, the redox shuttle mechanism is curtailed to a large degree. Deposition of insoluble sulphur species on the surface of the Li electrode and formation of irreversible Li_2S on the cathode surface are strongly inhibited. The last point is clearly demonstrated in SEM images of the PEG-functionalized CMK-3/S cathode before and after cycling, which exhibit very little change in surface morphology (Fig. 6), compared with CMK-3/S, which clearly shows precipitation of insoluble products on the surface of the mesoporous carbon particles.

In summary, we demonstrate that the strategy illustrated here provides a versatile route to nanostructured polymer-modified mesoporous carbon–sulphur composites that display all of the benefits of confinement effects at a small length scale. Intimate contact of the insulating sulphur and discharge-product sulphides with the retaining conductive carbon framework at nanoscale

dimensions affords excellent accessibility of the active material. The carbon framework not only acts as an electronic conduit to the active mass encapsulated within, but also serves as a mini-electrochemical reaction chamber. The entrapment ensures that a more complete redox process takes place, and results in enhanced utilization of the active sulphur material. This is vital to the success of all conversion reactions to ensure full reversibility of the back-reaction. The polymer coating on the external surface of the composite further helps retard diffusion of polysulphide out of the cathode structure, minimize the loss of the active mass in the cathode and improve the cycling stability. The composite materials reported here can supply up to nearly 80% of the theoretical capacity of sulphur (1,320 mA h g^{-1}), representing more than three times the energy density of lithium transition-metal oxide cathodes, at reasonable rates with good cycling stability. In our laboratory, mesoporous carbon frameworks with various wall thicknesses, conductivities and connectivities have recently been prepared to take advantage of structural and electronic variation of the constraining support. The three-dimensional variants such as CMK-1 and CMK-8 are particularly promising in this respect[42]. We will report those results in a forthcoming paper. Owing to the flexibility of the method, the high capacity of the carbon for active material incorporation and facile functionalization of the surface, we believe that a wide variety of nanostructured 'imbibed' composites could find broad application in many areas of materials science, not only as advanced electrode materials that rely on assimilation and conversion reactions.

Methods

Synthesis. For the synthesis of SBA-15 with controlled morphology[43], 2 g of Pluronic P123 ($EO_{20}PPO_{70}EO_{20}$) was dissolved in 60 ml of 2 M HCl at 38 °C. Tetraethylorthosilicate (4.2 g) was added to the above solution with vigorous stirring. The mixture was stirred for only 6 min and remained quiescent for 24 h at 38 °C. The mixture was subsequently heated at 100 °C for another 24 h in an autoclave. The as-synthesized SBA-15 with short-rod morphology was collected by filtration, dried and calcined at 550 °C in air. A nanocasting method was used to fabricate CMK-3 from SBA-15 as a hard template[44]. Sucrose (1.25 g) was dissolved in 5.0 ml of water containing 0.14 g H_2SO_4. Surfactant-free SBA-15 (1.0 g) was then dispersed in the above solution and the mixture was sonicated for 1 h; heated at 100 °C for 12 h and at 160 °C for another 12 h. The impregnation process was repeated once with another 5.0 ml aqueous solution containing 0.8 g sucrose and 0.09 g H_2SO_4. The composite was completely carbonized at 900 °C for 5 h in an argon atmosphere. To remove the SBA-15 silica template, the composite was stirred in a 5% HF solution at room temperature for 4 h, although NaOH can also be used to dissolve the silica.

The CMK-3/S nanocomposite was prepared following a melt-diffusion strategy. CMK-3 (1.0 g) and sulphur (2.33 g) were ground together, and heated to 155 °C. The weight ratio of sulphur/carbon was adjusted to be equal to or less than 7:3, to allow for expansion of the pore content on full lithiation to Li_2S. For example, 1.0 g of CMK-3 can accommodate 3.486 g of Li_2S (1.66 g cm^{-3} (density of Li_2S) × 2.1 cm^3 g^{-1}, the pore volume of the CMK-3), which corresponds to a maximum of 2.425 g of sulphur.

To prepare the CMK-3/S-PEG composite, CMK-3 was first functionalized with carboxylic groups by oxidization treatment in concentrated HNO_3 solution for half an hour at 80 °C, before incorporation of the sulphur. To tether the PEG chains to the surface of the CMK-3/S composite, the composite was dispersed in a PEG aqueous solution and the solution was heated at 58 °C and stirred continuously overnight to ensure complete reaction of the carboxylic groups on the carbon particles with the hydroxyl groups on the PEG. The mixture was sonicated for 20 min to completely remove physically absorbed PEG on the composite, and the CMK-3/S-PEG composite was collected by filtration and dried.

Characterization. X-ray diffraction patterns at low-angle (0.75° to 4° 2θ) and wide-angle (from 10° to 80° 2θ) were collected on a D8-ADVANCE powder X-ray diffractometer operating at 40 kV and 30 mA and using Cu-Kα radiation ($\lambda = 0.15406$ nm). Nitrogen adsorption and desorption isotherms were obtained using a Micromeritics Gemini 2735 system at −196 °C. Before measurement of CMK-3, the sample was degassed at 150 °C on a vacuum line following a standard protocol. It was not possible to carry this out for CMK-3/S owing to the volatility of the sulphur, and so no pretreatment was used. The BET method was used to calculate the surface area[45]. The total pore volumes were calculated from the amount adsorbed at a relative pressure of 0.99. The pore size distributions were calculated by means of the Barrett–Joyner–Halenda method applied to the desorption branch[46]. As the mesopores of CMK-3/S are decreased to micropores on (partial) filling with sulphur, the possibility of water entrapment, and/or pore blockage means that the values represent lower estimates.

The morphology of the sulphur/CMK-3 composites were examined by SEM using a LEO 1530 field-emission SEM instrument or a Hitachi S-5200 instrument. TEM was carried out on a Hitachi HD-2000 STEM. Conductivity measurements were carried out at room temperature using the four-point method. Sample bars for the measurement were cut from the pellets and then cold pressed using a force of 45 kN. Elemental analyses were carried out at M-H-W Laboratories, Phoenix, USA.

Electrochemistry. Positive electrodes were comprised 84 wt% CMK-3/S composite, 8 wt% Super-S carbon and 8 wt% poly(vinylidene fluoride) binder. The cathode materials were slurry-cast from cyclopentanone onto a carbon-coated aluminium current collector (Intelicoat). The electrolyte is composed of a 1.2 M $LiPF_6$ solution in ethyl methyl sulphone[47]. Lithium metal foil was used as the counter electrode. The equivalent current density for the 168 mA g^{-1} rate is 0.19 and 0.37 mA cm^{-2} for the 336 mA g^{-1} rate. To measure the degree of sulphur retention in the cathode, a 1.0 M $LiPF_6$ solution in TEGDME was used as the electrolyte. Cathodes comprising CMK-3/S-PEG were compared with simple mixtures of sulphur and acetylene black at the exact same S/C ratio. We used large Swagelok-type cells that accommodate a sufficient excess of the electrolyte to dissolve sulphur species. Swagelok cells were disassembled and immersed into TEGDME to completely extract sulphur species from the electrolyte. Sulphur analysis was carried out by Galbraith Laboratories (Tennessee, USA).

Received 10 September 2008; accepted 17 April 2009; published online 17 May 2009

References

1. Winter, M. & Brodd, R. Batteries, fuel cells and supercapacitors. *Chem. Rev.* **104**, 4245–4269 (2004).
2. Bruce, P. G. Energy storage beyond the horizon: Rechargeable lithium batteries. *Solid State Ion.* **179**, 752–760 (2008).
3. Rauh, R. D., Abraham, K. M., Pearson, G. F., Surprenant, J. K. & Brummer, S. B. A lithium/dissolved sulfur battery with an organic electrolyte. *J. Electrochem. Soc.* **126**, 523–527 (1979).
4. Shim, J., Striebel, K. A. & Cairns, E. J. The lithium/sulfur rechargeable cell. *J. Electrochem. Soc.* **149**, A1321–A1325 (2002).
5. Kang, K., Meng, Y. S., Bréger, J., Grey, C. P. & Ceder, G. Electrodes with high power and high capacity for rechargeable lithium batteries. *Science* **311**, 977–980 (2006).
6. Peled, E. & Yamin, H. Lithium/sulfur organic battery. *Prog. Batteries Sol. Cells* **5**, 56–58 (1984).
7. Chu, M.-Y. Rechargeable positive electrodes. US Patent US5686201 (1997).
8. Peramunage, D. & Licht, S. A solid sulfur cathode for aqueous batteries. *Science* **261**, 1029–1032 (1993).
9. Dean, J. A. (ed.) *Lange's Handbook of Chemistry* 3rd edn, 3–5 (McGraw-Hill, 1985).
10. Cunningham, P. T., Johnson, S. A. & Cairns, E. J. Phase equilibria in lithium–chalcogen systems: Lithium–sulfur. *J. Electrochem. Soc.* **119**, 1448–1450 (1972).
11. Choi, J.-W. *et al.* Rechargeable lithium/sulfur battery with suitable mixed liquid electrolytes. *Electrochim. Acta* **52**, 2075–2082 (2007).
12. Rauh, R. D., Shuker, F. S., Marston, J. M. & Brummer, S. B. Formation of lithium polysulfides in aprotic media. *J. Inorg. Nucl. Chem.* **39**, 1761–1766 (1977).
13. Cheon, S.-E. *et al.* Rechargeable lithium sulfur battery II. Rate capability and cycle characteristics. *J. Electrochem. Soc.* **150**, A800–A805 (2003).
14. Shin, J. H. & Cairns, E. J. Characterization of N-methyl-N-butylpyrrolidinium bis(trifluoromethanesulfonyl)imide-LiTFSI-tetra(ethylene glycol) dimethyl ether mixtures as a Li metal cell electrolyte. *J. Electrochem. Soc.* **155**, A368–A373 (2008).
15. Yuan, L. X. *et al.* Improved dischargeability and reversibility of sulfur cathode in a novel ionic liquid electrolyte. *Electrochem. Commun.* **8**, 610–614 (2006).
16. Ryu, H.-S. *et al.* Discharge behavior of lithium/sulfur cell with TEGDME based electrolyte at low temperature. *J. Power Sources* **163**, 201–206 (2006).
17. Wang, J. *et al.* Sulfur-mesoporous carbon composites in conjunction with a novel ionic liquid electrolyte for lithium rechargeable batteries. *Carbon* **46**, 229–235 (2008).
18. Chung, K.-I., Kim, W.-S. & Choi, Y.-K. Lithium phosphorous oxynitride as a passive layer for anodes in lithium secondary batteries. *J. Electroanal. Chem.* **566**, 263–267 (2004).
19. Visco, S. J., Nimon, Y. S. & Katz, B. D. Ionically conductive composites for protection of active metal anodes. US Patent 7,282,296, October 16 (2007).
20. Skotheim, T. A., Sheehan, C. J., Mikhaylik, Y. V. & Affinito, J. Lithium anodes for electrochemical cells. US patent 7247,408, July 24 (2007).
21. Akridge, J. R., Mikhaylik, Y. V. & White, N. Li/S fundamental chemistry and application to high-performance rechargeable batteries. *Solid State Ion.* **175**, 243–245 (2004).

22. Mikhaylik, Y. V. & Akridge, J. R. Low temperature performance of Li/S batteries. *J. Electrochem. Soc.* **150**, A306–A311 (2003).
23. Zheng, W., Liu, Y. W., Hu, X. G. & Zhang, C. F. Novel nanosized adsorbing sulfur composite cathode materials for the advanced secondary lithium batteries. *Electrochim. Acta* **51**, 1330–1335 (2006).
24. Cheon, S.-E. *et al.* Capacity fading mechanisms on cycling a high-capacity secondary sulfur cathode. *J. Electrochem. Soc.* **151**, A2067–A2073 (2004).
25. Song, M.-S. *et al.* Effects of nanosized adsorbing material on electrochemical properties of sulfur cathode for Li/S secondary batteries. *J. Electrochem. Soc.* **151**, A791–A795 (2004).
26. Kobayashi, T. *et al.* All solid-state battery with sulfur electrode and thio-LISICON electrolyte. *J. Power Sources* **182**, 621 (2008).
27. Wang, J., Yang, J., Xie, J. & Xu, N. A novel conductive polymer-sulfur composite cathode material for rechargeable lithium batteries. *Adv. Mater.* **14**, 963–965 (2002).
28. Ryoo, R., Joo, S. H. & Jun, S. Synthesis of highly ordered carbon molecular sieves via template mediated structural transformations. *J. Phys. Chem. B* **103**, 7743–7746 (1999).
29. Lee, J., Kim, J. & Hyeon, T. Recent progress in the synthesis of porous carbon materials. *Adv. Mater.* **18**, 2073–2094 (2006).
30. Jiao, F. & Bruce, P. G. Mesoporous crystalline β-MnO_2—a reversible positive electrode for rechargeable lithium batteries. *Adv. Mater.* **19**, 657–660 (2007).
31. Jiao, F., Shaju, K. M. & Bruce, P. G. Synthesis of nanowire and mesoporous low-temperature $LiCoO_2$ by a post-templating reaction. *Angew. Chem. Int. Ed.* **117**, 6708–6711 (2005).
32. Ji, X., Herle, P. S., Rho, Y. H. & Nazar, L. F. Carbon/MoO_2 composite based on porous semi-graphitized nanorod assemblies from in situ reaction of tri-block polymers. *Chem. Mater.* **19**, 374–383 (2007).
33. Grigoriants, I. *et al.* The use of tin-decorated mesoporous carbon as an anode material for rechargeable lithium batteries. *Chem. Commun.* 921–923 (2005).
34. Joo, S. *et al.* Ordered nanoporous arrays of carbon supporting high dispersions of platinum nanoparticles. *Nature* **412**, 169–172 (2001).
35. Ryoo, R., Joo, S., Kruk, M. & Jaroniec, M. Ordered mesoporous carbons. *Adv. Mater.* **13**, 677–681 (2001).
36. Lei, J. *et al.* Immobilization of enzymes in mesoporous materials: Controlling the entrance to nanospace. *Micropor. Mesopor. Mater.* **73**, 121–128 (2004).
37. Miessler, G. L. & Tarr, D. A. *Inorganic Chemistry* (Pearson Education, 1998).
38. Landau, M. V., Vradman, L., Wang, X. & Titelman, L. High loading TiO_2 and ZrO_2 nanocrystals ensembles inside the mesopores of SBA-15: Preparation, texture and stability. *Micropor. Mesopor. Mater.* **78**, 117–129 (2005).
39. Kim, J., Lee, J. & Hyeon, T. Direct synthesis of uniform mesoporous carbons from the carbonization of as-synthesized silica/triblock copolymer nanocomposites. *Carbon* **42**, 2711–2719 (2004).
40. Yamin, H., Gorenshtein, A., Penciner, J., Sternberg, Y. & Peled, E. Lithium sulfur battery. Oxidation/reduction mechanisms of polysulfides in THF solutions. *J. Electrochem. Soc.* **135**, 1045–1048 (1988).
41. Kumaresan, K., Mikhaylik, Y. & White, R. E. A mathematical model for a lithium–sulfur cell. *J. Electrochem. Soc.* **155**, A576–A582 (2008).
42. Gierszal, K. P., Kim, T.-W., Ryoo, R. & Jaroniec, M. Adsorption and structural properties of ordered mesoporous carbons synthesized by using various carbon precursors and ordered siliceous *P6mm* and *Ia3hd* mesostructures as templates. *J. Phys. Chem. B* **109**, 23263–23268 (2005).
43. Yu, C., Fan, J., Tian, B. & Zhao, D. Morphology development of mesoporous materials: A colloidal phase separation mechanism. *Chem. Mater.* **16**, 889–898 (2004).
44. Jun, S. *et al.* Synthesis of new, nanoporous carbon with hexagonally ordered mesostructure. *J. Am. Chem. Soc.* **122**, 10712–10713 (2000).
45. Brunauer, S., Emmett, P. H. & Teller, E. Adsorption of gases in multimolecular layers. *J. Am. Chem. Soc.* **60**, 309–319 (1938).
46. Barrett, E. P., Joyner, L. G. & Halenda, P. P. The determination of pore volume and area distributions in porous substances. I. Computations from nitrogen isotherms. *J. Am. Chem. Soc.* **73**, 373–380 (1951).
47. Xu, K. & Angell, C. A. High anodic stability of a new electrolyte solvent: Unsymmetric noncyclic aliphatic sulfone. *J. Electrochem. Soc.* **145**, L70–L72 (1998).

Acknowledgements

NSERC is gratefully acknowledged for financial support. We thank N. Coombs, University of Toronto, for help with acquisition of the TEM and SEM images.

Additional information

Supplementary information accompanies this paper on www.nature.com/naturematerials. Reprints and permissions information is available online at http://npg.nature.com/reprintsandpermissions. Correspondence and requests for materials should be addressed to L.F.N.